AIAA AVIATION Forum
12-16 June 2023, San Diego, CA and Online
AIAA AVIATION 2023 Forum

10.2514/6.2023-4351

Self-consistent closure modeling for linearized mean field methods

Jakob G. R. von Saldern *, Johann Moritz Reumschüssel †, Thomas L. Kaiser ‡, Oliver T. Schmidt §, Peter Jordan ¶, and K. Oberleithner ‖

Institute of Fluid Dynamics and Technical Acoustics, Technische Universität Berlin, Berlin, Germany
Mechanical and Aerospace Engineering, University of California, San Diego, La Jolla, CA 92093, USA
Institut Pprime, CNRS / Université de Poitier / ENSMA, 86962 Futuroscope Chasseneuil, France

Modeling the coherent component of the Reynolds stresses to close the linearized mean field equations has received little attention in recent years, despite the great surge of linearized mean field methods. In this study, we present a modeling approach to account for the coherent component of the Reynolds stresses that is based on a Boussinesq-like model known from steady and unsteady Reynolds-averaged Navier Stokes (RANS) equations. The presented approach is based on two features. Unlike many previous studies, we consider not only a mean eddy viscosity field, but also a fluctuating field derived from linearized algebraic models. Moreover, we introduce the concept of mean field consistency; the mean eddy viscosity field is determined to satisfy the RANS equations along with the other mean field quantities. Practically, this is implemented by assimilating the model constants of the eddy viscosity model from the mean fields, taking into account the RANS equations, which is achieved with a physics-informed neural network. To evaluate the models thus assembled, we propose to perform an a priori analysis. A concept in which the modeled Reynolds stress fluctuations are directly compared to the respective measured quantities. The proposed methods are demonstrated and evaluated on a jet flow at Reynolds number of 50000 and Mach number 0.4.

I. Introduction

Linearized mean field methods are emerging in the field of computational fluid dynamics. They are based on a linear flow operator that can be derived by linearizing the governing flow equations around the temporal mean. This linear operator can be used for a variety of applications, such as analyzing, predicting, and suppressing the dominant flow dynamics. The analysis of fluid dynamics based on the base flow is a long-established method. However, the use of the temporal mean field as the basis for linearization is much less established. Barkley has used linearized mean field methods to study the dynamics of a cylinder wake [1]. Building on this, the methodology has been used by a wide range of scientists for both academic and industrial applications. Fields of application include isothermal, swirling [2], and reacting flows [3–6], high-enthalpy jets [7], prediction of jet noise [8] and trailing edge noise from airfoils [9–11], hydroturbines [12, 13], and more.

Using the temporal mean as a linearization basis, however, also introduces major difficulties related to the commonly known turbulence closure model; the operator linearized around the mean field contains the coherent Reynolds stresses, whose modeling is still in the initial stage [14–18]. The most common modeling approach is to use a linearized Boussinesq-like turbulence model that relates the coherent Reynolds stresses to two terms; first, a mean eddy viscosity combined with a fluctuating shear stress tensor and second, a fluctuating eddy viscosity combined with a mean shear stress tensor. While this approach significantly reduces the number of quantities to be modeled, it presents two additional challenges. First, this approach requires a mean eddy viscosity field, which is generally unknown for high-fidelity mean field data, such as mean fields obtained by time averaging large-eddy simulation (LES) or particle image velocimetry (PIV) snapshots. Second, a model for the eddy viscosity fluctuations is needed. Whereas the modeling of the fluctuating eddy viscosity has been neglected up to now, with a few exceptions [19, 20], the first term is typically taken into account via mean eddy viscosity fields calibrated to the high fidelity mean field or ad hoc approaches based on constant fields.

*PhD candidate, Laboratory for Flow Instabilities and Dynamics, j.vonsaldern@tu-berlin.de
†PhD candidate, Chair of Fluid Dynamics, m.reumschuessel@tu-berlin.de
‡PostDoc Fellow, Laboratory for Flow Instabilities and Dynamics, t.kaiser@tu-berlin.de
§Professor, Mechanical and Aerospace Engineering, University of California, San Diego, La Jolla, CA 92093, USA
¶Professor, Institut Pprime, CNRS / Université de Poitiers / ENSMA, 86962 Futuroscope Chasseneuil, France
‖Professor, Laboratory for Flow Instabilities and Dynamics, oberleithner@tu-berlin.de

Under the constraint of low rank dynamics, the dominant structures in a flow can be modeled via a resolvent analysis of the linear operator [21]. Driven by the goal of obtaining the best possible agreement in this respect, finding a closure model for the coherent Reynolds stress tensor has received much more attention in the recent past. For example, the energy transfer of turbulent scales in a channel flow has been intensively studied by Symon et al. to draw conclusions on the modeling of the coherent Reynolds stresses [17, 18]. It was found that an eddy viscosity model primarily removes energy, which makes the model less applicable for scales that receive energy through the coherent Reynolds stress term. In a study by Kuhn et al. it was found that the coherent Reynolds stress tensor in the far field of a jet can be well approximated by a spatially constant eddy viscosity retrieved from the mean velocity field [15, 16]. By matching SPOD modes with resolvent modes, Pickering et al. determine optimal eddy viscosity fields for jet flows at subsonic and supersonic conditions [14]. However, the use of eddy viscosity fields obtained from SPOD data or calculated from LES mean fields by inverting the Boussinesq model usually results in inconsistency of the mean fields: the high fidelity mean fields, together with the mean eddy viscosity field, do not satisfy the Reynolds-averaged Navier Stokes (RANS) equations. In other words, the set of mean fields do not satisfy the equations from which the linearized equations are derived.

In this study, we propose a mean-field consistent linear model of the coherent component of the Reynolds stresses. The consistency of the mean field is achieved by assimilating the parameters of the eddy viscosity model from the high-fidelity mean fields using the method of physics-informed neural network (PINN), which allows the inclusion of the RANS equations as an additional constraint in the assimilation process. As a result, the high-fidelity mean fields together with the assimilated eddy viscosity field satisfy the RANS equations and are thus consistent with the linearized operator. In contrast to most other studies, fluctuations in eddy viscosity are accounted for by linearization of an algebraic eddy viscosity model. The effectiveness of this new class of coherent Reynolds stresses is investigated by comparing the model against the coherent component of Reynolds stresses retrieved from stochastically (turbulent) forced jet LES data. In addition, resolvent modes for selected eddy viscosities are compared with SPOD modes.

The study is structured as follows. In the first part, we introduce the equations, define the problem of closing the linear equations, and present our modeling approach. In the second part, other methodologies used for data analysis and evaluation of modeling are explained. In the third part, the modeling approach is applied to a jet flow at a Reynolds number of 50000 and a Mach number of 0.4.

II. Self-consistent closure modeling

A. Mean field equations

The triple decomposition allows the flow variables to be decomposed into a time-averaged component, a coherent component, and a stochastic component. In the following they are denoted with an over-line, a tilde and two dash symbols, respectively, e. g. the velocity vector reads $\mathbf{u} = \overline{\mathbf{u}} + \widetilde{\mathbf{u}} + \mathbf{u}''$. Inserting this ansatz into the Navier Stokes equations and time averaging yields the RANS equations

$$(\overline{\mathbf{u}} \cdot \nabla)\overline{\mathbf{u}} = -\frac{1}{\rho}\nabla\overline{p} + \nu\nabla^2\overline{\mathbf{u}} - \nabla \cdot \underbrace{\left(\overline{\widetilde{\mathbf{u}}\widetilde{\mathbf{u}}} + \overline{\mathbf{u}''\mathbf{u}''}\right)}_{\overline{\mathbf{R}}}, \tag{1}$$

where $\overline{\mathbf{R}}$ is the Reynolds stress tensor that has to be modeled in order to solve the RANS equations as a boundary value problem. The most common model is the Boussinesq approach that relates the deviatoric part of the Reynolds stress tensor to the mean strain rate tensor $\overline{\mathbf{T}}$

$$\overline{\mathbf{D}} \equiv \overline{\mathbf{R}} - \frac{2}{3}\overline{k}\mathbf{I} \approx -\overline{\nu}_t \underbrace{[\nabla + \nabla^T]\overline{\mathbf{u}}}_{\overline{\mathbf{T}}}, \tag{2}$$

where $\overline{k} = 1/2\,\mathrm{Tr}(\overline{\mathbf{R}})$ is the turbulent kinetic energy, $\mathbf{I}$ is the identity matrix and $\overline{\nu}_t$ is the mean eddy viscosity that has to be modeled with an appropriate closure model in order to solve the set of mean flow equations. Inserting the Boussinesq model into Eq. (1) yields

$$(\overline{\mathbf{u}} \cdot \nabla)\overline{\mathbf{u}} + \frac{1}{\rho}\nabla\overline{q} - \nabla \cdot \left[(\nu + \overline{\nu}_t)[\nabla + \nabla^T]\overline{\mathbf{u}}\right] = \overline{\mathbf{f}}, \tag{3}$$

where $\overline{q} = \overline{p} + 2/3\rho\overline{k}$ is the modified mean pressure and $\overline{\mathbf{f}}$ is the residual consisting of mean momentum transfer that is not captured with the Boussinesq model. When solving the RANS equations as a boundary value problem, it is assumed that the Reynolds stress tensor is correctly represented with the eddy viscosity model, i.e. $\overline{\mathbf{f}} = \mathbf{0}$.

B. Transport of coherent fluctuations

If instead of time averaging an ensemble average is performed after inserting the triple decomposition into the Navier Stokes equations the unsteady Reynolds-averaged Navier Stokes (URANS) equations can be derived

$$\frac{\partial\langle\mathbf{u}\rangle}{\partial t} + (\overline{\mathbf{u}}\cdot\nabla)\overline{\mathbf{u}} + (\widetilde{\mathbf{u}}\cdot\nabla)\overline{\mathbf{u}} + \overline{\mathbf{u}}\cdot\nabla\overline{\mathbf{u}} = -\frac{1}{\rho}\nabla\langle p\rangle + \nu\nabla^2\langle\mathbf{u}\rangle - \nabla\cdot(\langle\widetilde{\mathbf{u}}\widetilde{\mathbf{u}}\rangle + \underbrace{\langle\mathbf{u}''\mathbf{u}''\rangle}_{\langle\mathbf{R}\rangle}), \tag{4}$$

where $\langle\cdot\rangle$ denotes the ensemble average, extracting the deterministic part of a quantity, e.g. $\langle u\rangle = \overline{u} + \widetilde{u}$. The last term of Eq. (4), here referred to as the ensemble-averaged Reynolds stress term, must be modeled in order to close the URANS equations. This is typically achieved by applying a Boussinesq-like model that relates its deviatoric part to the ensemble average of the strain rate tensor

$$\langle\mathbf{D}\rangle = \langle\mathbf{R}\rangle - \frac{2}{3}\langle k\rangle\mathbf{I} \approx -\langle\nu_t\rangle[\nabla + \nabla^T]\langle\mathbf{u}\rangle \tag{5}$$

By subtracting the RANS equations, Eq. (1) from the URANS equations, Eq. (4), a transport equations for the coherent quantities can be derived

$$\frac{\partial\widetilde{\mathbf{u}}}{\partial t} + (\overline{\mathbf{u}}\cdot\nabla)\widetilde{\mathbf{u}} + (\widetilde{\mathbf{u}}\cdot\nabla)\overline{\mathbf{u}} = -\frac{1}{\rho}\nabla\widetilde{p} + \nu\nabla^2\widetilde{\mathbf{u}} - \nabla\cdot(\widetilde{\widetilde{\mathbf{u}}\widetilde{\mathbf{u}}} + \underbrace{\widetilde{\mathbf{u}''\mathbf{u}''}}_{\widetilde{\mathbf{R}}}). \tag{6}$$

Equation (6) is the basis for linearized mean field methods. The second last nonlinear term represents the interaction of the coherent structure with itself and is of higher order. The last term $\widetilde{\mathbf{R}}$ is the coherent component of the Reynolds stress tensor and is of the same order as the coherent fluctuations [22]. Its deviatoric part can be computed by subtracting Eq. (2) from Eq. (5) and neglecting higher order terms [20]

$$\widetilde{\mathbf{D}} \equiv \widetilde{\mathbf{R}} - \frac{2}{3}\widetilde{k}\mathbf{I} = \langle\mathbf{D}\rangle - \overline{\mathbf{D}} \approx -\overline{\nu}_t[\nabla + \nabla^T]\widetilde{\mathbf{u}} - \widetilde{\nu}_t[\nabla + \nabla^T]\overline{\mathbf{u}} = -\overline{\nu}_t\widetilde{\mathbf{T}} - \widetilde{\nu}_t\overline{\mathbf{T}} \tag{7}$$

Equation (7) relates the coherent component of the Reynolds stresses to two terms; a mean eddy viscosity times the coherent strain rate tensor and a coherent eddy viscosity times the mean strain rate tensor. Choosing an harmonic ansatz for the coherent fluctuations $\widetilde{\mathbf{x}} = \Re\{\widehat{\mathbf{x}}\exp(i\omega t)\}$ yields the Boussinesq-like model in frequency space

$$\widehat{\mathbf{D}} = -\overline{\nu}_t[\nabla + \nabla^T]\widehat{\mathbf{u}} - \widehat{\nu}_t[\nabla + \nabla^T]\overline{\mathbf{u}} = -\overline{\nu}_t\widehat{\mathbf{T}} - \widehat{\nu}_t\overline{\mathbf{T}}. \tag{8}$$

Inserting the harmonic ansatz and the closure model into Eq. (6) yields the transport equations of harmonic fluctuations

$$i\omega\widehat{\mathbf{u}} + (\overline{\mathbf{u}}\cdot\nabla)\widehat{\mathbf{u}} + (\widehat{\mathbf{u}}\cdot\nabla)\overline{\mathbf{u}} + \frac{1}{\rho}\nabla\widehat{q} - \nabla\cdot\left[(\nu + \overline{\nu}_t)[\nabla + \nabla^T]\widehat{\mathbf{u}} - \widehat{\nu}_t[\nabla + \nabla^T]\overline{\mathbf{u}}\right] = \widehat{\mathbf{f}}, \tag{9}$$

where $\widehat{q} = \widehat{p} + 2/3\rho\widehat{k}$ is the modified harmonic pressure and the vector $\widehat{\mathbf{f}}$ contains remaining (nonlinear) terms that are not captured by the eddy viscosity model. For the sake of completeness, the corresponding continuity equation is also given:

$$\nabla\cdot\widehat{\mathbf{u}} = 0. \tag{10}$$

When modeling the coherent Reynolds stress tensor, the influence of the fluctuating eddy viscosity is usually neglected. The mean eddy viscosity derived from the mean fields is usually positive. Considering the energy transfer of the coherent scales [17, 18], it becomes evident that a positive eddy viscosity primarily represents the dissipative part of the nonlinear transfer of the coherent structures. Modeling the coherent Reynolds stress term with only a mean eddy viscosity term therefore limits the modeling to structures that primarily transfer energy to other scales.

C. Eddy viscosity model

It is well known that considering a mean eddy viscosity to model the coherent Reynolds stress tensor (Eq. (8)) improves the predictions of linear methods [2, 16, 19, 23]. The most common approach to determine an eddy viscosity for a given flow field is to invert the Boussinesq model, Eq. (2)

$$\overline{\nu}_t = \frac{\langle \overline{\mathbf{D}}, -\overline{\mathbf{T}} \rangle_F}{\langle \overline{\mathbf{T}}, \overline{\mathbf{T}} \rangle_F}, \tag{11}$$

where the operation $\langle \mathbf{A}, \mathbf{B} \rangle_F = \sum_l A_l B_l^*$ denotes the Frobenius inner product between tensor $\mathbf{A}$ and $\mathbf{B}$. The symbol $*$ denotes the complex conjugate, which can be ignored here, since the mean flow quantities are real valued. The sum is over all components of the tensors. Equation (11) corresponds to a least squares fit considering all components of the deviatoric part of the Reynolds stress tensor. Mean eddy viscosities computed with Eq. (11) are referred to as least squares eddy viscosity, $\overline{\nu}_t$LSQ, in the following. The advantage of this approach is that a mean eddy viscosity can be calculated directly from the Reynolds stress tensor and given mean velocity fields. However, the least squares approximation often results in noisy fields, requiring post-processing to smooth the result. In addition, the method weights all terms equally, so that no distinction is made as to which terms are particularly important for the mean momentum transfer. In particular, this also leads to an inconsistency of the mean fields; the mean flow quantities together with the mean eddy viscosity do not represent a solution of the RANS equations, Eq. (3). A method to determine a suitable eddy viscosity based only on the mean field, without having to consider turbulent statistics and their spatial derivatives would be advantageous.

To provide self-consistency of the mean fields and to avoid noisy gradients, we propose the use of an eddy viscosity model whose constants are assimilated based on the mean velocity fields considering the RANS equations. The use of an eddy viscosity model allows furthermore to take into account a fluctuating component by linearizing the eddy viscosity model around the mean field [20]. For the sake of simplicity, an algebraic Prandtl mixing length model is used [24], reading

$$\nu_t(\langle \mathbf{u} \rangle) = l_m^2 \left| \frac{\partial \langle u_x \rangle}{\partial r} \right|, \tag{12}$$

where l_m is the mixing length. Based on a linearization around the temporal mean the eddy viscosity model can be decomposed into a mean and a coherent part [20], $\nu_t = \overline{\nu}_t + \tilde{\nu}_t$, where

$$\overline{\nu}_t = l_m^2 \left| \frac{\partial \overline{u}_x}{\partial r} \right| \tag{13}$$

$$\widehat{\nu}_t = l_m^2 \mathrm{sign}\left(\frac{\partial \overline{u}_x}{\partial r} \right) \frac{\partial \widehat{u}_x}{\partial r}. \tag{14}$$

In Eq. (14), an harmonic ansatz is used for the coherent quantities. With Eqs. (13) and (14) the coherent part of the Reynolds stress tensor can be related to mean and coherent velocity components (Eq. (8)).

As introduced above, for the sake of mean field consistency the mixing length l_m is assimilated from the LES mean fields taking into account the RANS equations. The assimilation is performed using a PINN. For this purpose the mean field quantities in Eq.(3), modified mean pressure, velocity components and the mixing length are approximated with a neural network $\mathbf{F}_\alpha$; the neural network maps spatial coordinates to the mean field quantities

$$[\overline{\mathbf{u}},\ \overline{q},\ l_m] = \mathbf{F}_\alpha(x, r). \tag{15}$$

The parameters of the neural network α are found by minimizing a composite loss function that includes given mean fields from the LES, $\overline{\mathbf{u}}_{\mathrm{LES}}$ and $\overline{q}_{\mathrm{LES}}$, and the residual of the RANS equations $\overline{\mathbf{f}}_\alpha$, Eqs. (3). Using the composite loss function ensures that both the high-fidelity LES mean fields are approximated as good as possible and a mixing length (and with Eq. (13) mean eddy viscosity) is assimilated that, together with the mean fields, satisfies the time-averaged equations as good as possible. More details on the methodology, network design and training algorithms can be found in our recent publication on mean field data assimilation with PINN [25] or in the original publication of the methodology [26]. The mean eddy viscosity determined with the assimilated mixing length, Eq. (13), is referred to as PINN eddy viscosity in the following.

Finally, Eq. (8) will be considered again, which relates the deviatoric component of the coherent Reynolds stress tensor to the coherent shear stress tensor via the eddy viscosity. If the coherent quantities are known, in analogy to

the inversion of the Boussinesq equation (Eq. 11), the Boussinesq-like model can also be inverted. If the fluctuating component of the eddy viscosity is negligible, the mean eddy viscosity can be determined as follows

$$\overline{\nu}_t \approx \frac{\langle \widehat{\mathbf{D}}, -\widehat{\mathbf{T}} \rangle_F}{\langle \widehat{\mathbf{T}}, \widehat{\mathbf{T}} \rangle_F} \tag{16}$$

This way of calculating the mean eddy viscosity again corresponds to a least-squares fit, but in contrast to Eq. (11), based on the fluctuating and not the mean quantities, Eq. (8). At this point, it should be noted that the use of a mean eddy viscosity to model the deviatoric component of the coherent Reynolds stress tensor based on the coherent strain rate tensor is a modeling assumption. The inversion of the corresponding model on the basis of given coherent quantities allows to determine an optimal eddy viscosity in the least squares sense. A comparison with the commonly used LSQ or PINN mean eddy viscosity can thus provide information on the potential of the quantities to approximate the closure term. It should be noted, however, that the coherent fields are complex-valued and frequency dependent.

III. Methodology

This section briefly introduces the methods used in the study. These are the modeling of coherent structures based on resolvent analysis and the empirical determination of coherent structures using SPOD. The natural flow of a jet at a Reynolds number of 50000 and a Mach number of 0.4 is used as the data set, generated using a large-eddy simulation based on the flow solver 'Charles' [27, 28]. The LES geometry is based on an experimental setup. For more information on the experiments and computations, please refer to the following studies [29, 30].

A. Resolvent analysis

With a given eddy viscosity model, the governing transport equations of harmonic fluctuations, Eqs. (9) and (10), can be rearranged in the form

$$\left[\widehat{\mathbf{u}}_m, \widehat{q}_m\right]^T = \underbrace{\left(i\omega \mathbf{B}_m - \mathbf{L}_m\right)^{-1}}_{\mathcal{R}(i\omega)} \widehat{\mathbf{f}}, \tag{17}$$

where $\mathbf{B}$ and $\mathbf{L}$ are linear operators. Please note that we consider cylindrical coordinates and axis symmetry. Hence, with an harmonic ansatz in the azimuthal direction $\widehat{\mathbf{x}}(x, r, \theta) \rightarrow \widehat{\mathbf{x}}(x, r) \mathrm{e}^{im\theta}$, the problem simplifies into two spatial dimensions for each given azimuthal wavenumber m. This implies, however, that the linear operators change with the azimuthal order m.

The operator $\mathcal{R}(i\omega)$ is known as the resolvent operator. In resolvent analysis, the exact interpretation of $\widehat{\mathbf{f}}$ is of secondary importance. The goal of the analysis is to find out which dynamics in the flow is most strongly excited by linear mechanisms and how the corresponding structure of the best excitation is. Therefore, $\widehat{\mathbf{f}}$ is to be understood as a body forcing term, which can excite the flow in form of an harmonic forcing anywhere in the domain. A singular value decomposition of the resolvent operator yields

$$\mathcal{R} = \mathbf{U}\mathbf{\Sigma}\mathbf{V}^*, \tag{18}$$

where the matrix $\mathbf{\Sigma}$ contains the singular values that are called resolvent gains in this context. The matrices $\mathbf{V}$ and $\mathbf{U}$ contain the forcing and response modes, respectively. Multiplying Eq. (18) with $\mathbf{V}$ and considering one mode pair j illustrates the understanding of forcing and response modes

$$\mathcal{R}\mathbf{v}_j = \sigma_j \mathbf{u}_j. \tag{19}$$

The mode $\mathbf{u}_j$ is the response to the forcing $\mathbf{v}_j$ where σ_j denotes the corresponding gain amplification. Considering a natural flow without external excitation, the response mode corresponding to the largest resolvent gain can be understood as the coherent structure of the flow that is most amplified due to linear mechanisms. Since this is the most amplified dynamics and the flow is excited everywhere by background turbulence, it can be assumed that the leading response mode can be observed in a natural flow.

B. Spectral proper orthogonal decomposition

To extract coherent structures from the natural flow data the method of spectral proper orthogonal decomposition (SPOD) is applied. In frequency bands with large gain separation the corresponding SPOD modes can be considered as

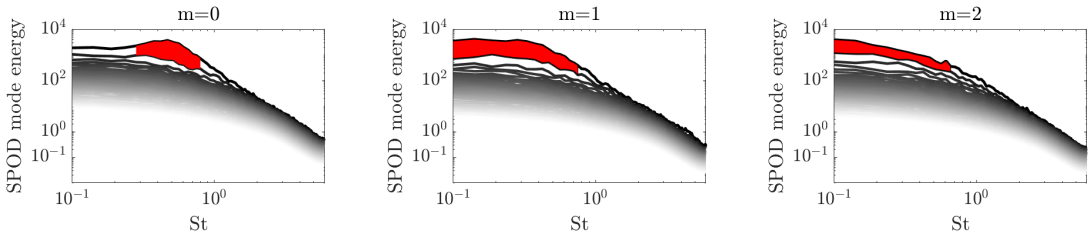

(a) m=0 **(b) m=1** **(c) m=2**

Fig. 1 SPOD spectra for m=0, 1 and 2. The frequency ranges of high gain separation are highlighted in red.

coherent structures. If the underlying mechanism is linear the structure is typically captured with a resolvent analysis [21]. Thus, it is common to validate the resolvent modes in frequency ranges with high gain seperation with the corresponding SPOD modes. Or, in other words, resolvent analysis attempts to model the coherent structures observed with SPOD. In the scope of this study coherent structures of different azimuthal orders are considered. For this purpose, the velocity fluctuations $\mathbf{u}' = \mathbf{u} - \overline{\mathbf{u}}$ are first azimuthally decomposed

$$\widehat{\mathbf{u}}_m(x, r, t) = \int_0^{2\pi} \mathbf{u}'(x, r, \theta, t) \mathrm{e}^{-im\theta} \mathrm{d}\theta, \tag{20}$$

where x, r, θ and t are the axial, radial and azimuthal coordinate and time respectively. Subsequently, the time series for each azimuthal order $m = 0, 1, 2$ are considered separately. The time series for a given azimuthal mode number is decomposed into segments of 256 snapshots and each segment is transformed into frequency space using a temporal Fourier transform. Subsequently, a proper orthogonal decomposition (POD) is performed for each frequency ω. For this purpose, the cross-spectral density matrix is calculated first, whose entries (l, k) are as follows

$$C^{l,k}_{m,\omega} = \frac{1}{N} \int_\Omega (\widehat{\mathbf{u}}^l_{m,\omega})^* \, \widehat{\mathbf{u}}^k_{m,\omega} \mathrm{d}\Omega, \tag{21}$$

where Ω denotes the domain and N the number of blocks. The superscripts l and k denote the block number. The spectral POD modes follow from solving the eigenvalue problem

$$\mathbf{C}_{m,\omega} \mathbf{a}^j_{m,\omega} = \lambda^j \mathbf{a}^j_{m,\omega} \tag{22}$$

and projecting back the Fourier coefficients onto the eigenvectors

$$\widehat{\mathbf{u}}^j_{\mathrm{SPOD},m,\omega} = \frac{1}{N} \sum_{k=1}^{N} \mathbf{a}^j_{m,\omega} \widehat{\mathbf{u}}^k_{m,\omega}, \tag{23}$$

where the superscript j denotes the considered mode number. The sum represents an average over all N blocks. The magnitude of the corresponding eigenvalue λ^j represents the kinetic energy associated with the corresponding SPOD mode, which allows to rank the SPOD modes by energy content for each frequency. In the scope of this study we are mostly interested in the leading mode ($j = 1$) that corresponds to the coherent structure with the highest energy content.

In addition to the SPOD velocity modes the extended spectral proper orthogonal decomposition (eSPOD) modes of the coherent component of the Reynolds stress tensor are computed. The eSPOD allows to compute the part of a signal that correlates with the SPOD modes. For this purpose the fluctuating Reynolds stress tensor $\mathbf{R}' = \mathbf{u}' \otimes \mathbf{u}'$ is decomposed in azimuthal waves of order m

$$\widehat{\mathbf{R}}_m(x, r, t) = \int_0^{2\pi} \mathbf{R}'(x, r, \theta, t) \mathrm{e}^{-im\theta} \mathrm{d}\theta, \tag{24}$$

split in N blocks and transformed in frequency space. The resulting azimuthal and frequency decomposed coherent Reynolds stress tensor is projected on the SPOD eigenvectors to extract the part that correlates with the velocity fluctuations

$$\widehat{\mathbf{R}}^j_{\mathrm{eSPOD},m,\omega} = \frac{1}{N\lambda^j} \sum_{k=1}^{N} \mathbf{a}^j_{m,\omega} \widehat{\mathbf{R}}^k_{m,\omega}. \tag{25}$$

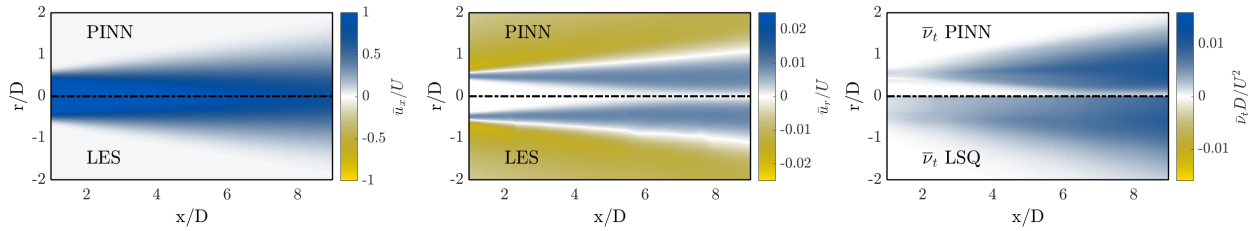

(a) axial velocity **(b) radial velocity** **(c) mean eddy viscosity**

Fig. 2 LES and PINN assimilated mean flow quantities

In the following, hat-symbols of velocities represent SPOD and of Reynolds stress components eSPOD modes - the indices eSPOD, SPOD, m and ω are omitted. Moreover, in the context of this study only modes of leading order are considered ($j = 1$).

Figure 1a, 1b and 1c show the SPOD spectra for $m = 0, 1$ and 2, respectively. The Strouhal number is defined as $\mathrm{St} = fD/U$, where D is the nozzle diameter and U is the bulk velocity. A region of high gain separation is observed for all three azimuthal wavenumbers, although the corresponding frequency ranges in which the separation occurs are different. For $m = 0$ the leading mode clearly dominates the dynamics for $\mathrm{St} \in [0.28, 0.65]$, for $m = 1$ for $\mathrm{St} \in [0.1, 0.75]$ and for $m = 2$ for $\mathrm{St} \in [0.1, 0.65]$. The regions of high gain separation are marked in red in Fig. 1. In these regions of low-rank dynamics, the flow is dominated by coherent structures; the goal of the resolvent analysis is to model these structures.

IV. Results

In the following, the LES mean fields, the PINN assimilation results, as well as mean eddy viscosity fields are presented first. In the second part, the potential of different eddy viscosities to model the deviatoric part of the coherent Reynolds stress tensor is investigated using a priori analysis, a concept that evaluates the model in isolation. Finally, resolvent modes based on different mean eddy viscosities are computed and compared with the respective empirical SPOD modes.

A. Mean fields

The lower halves of Fig. 2a and 2b show the mean axial and mean radial velocity components respectively, computed by time averaging the LES snapshots in the region $x/D \in [1, 9]$ and $r/D \in [0, 2]$. The lower half of Fig. 2c shows the LSQ eddy viscosity computed based on the mean velocity fields and the inversion of the Boussinesq model, Eq. (11). To reduce noise introduced by the inversion of the Boussinesq model, the eddy viscosity field is smoothed with a moving average filter. The upper halves in Fig. 2 show the respective approximations using the PINN. Please note that the PINN maps the spatial coordinates to the mean axial and radial velocity component, the mean modified pressure and the mixing length. The corresponding PINN eddy viscosity is computed using the assimilated mixing length and the gradient of the mean velocity field, Eq. (13). The mean velocity components are very well approximated by the PINN. The modified mean pressure, which is also included in the PINN training, is not shown for brevity, but the PINN approximation for this component is as good as for the mean velocity components. Qualitatively, the PINN eddy viscosity looks similar to the LSQ eddy viscosity. Clear differences can be seen in the region of the potential core, where the PINN eddy viscosity is significantly lower compared to the one based on the Boussinesq inversion. The differences stem from the fact that the PINN eddy viscosity is determined in accordance with the RANS equations and thus is mean field consistent, unlike the LSQ eddy viscosity.

According to the Boussinesq model, Eq. (2), the eddy viscosity together with the mean strain rate tensor are supposed to model the deviatoric part of the mean Reynolds stress tensor. This capability can be evaluated by comparing the modeled Reynolds stress components based on the two mean eddy viscosity fields with the corresponding components obtained by averaging LES snapshots. For this purpose, the two eddy viscosity fields together with the mean velocity fields are substituted into the Boussinesq equation, Eq. (2), which yields the modeled Reynolds stresses. The PINN and LSQ eddy viscosities are evaluated using the respective PINN and LES mean velocity fields. However, since the PINN approximates the mean fields very well, it can be assumed that the two velocity fields are identical.

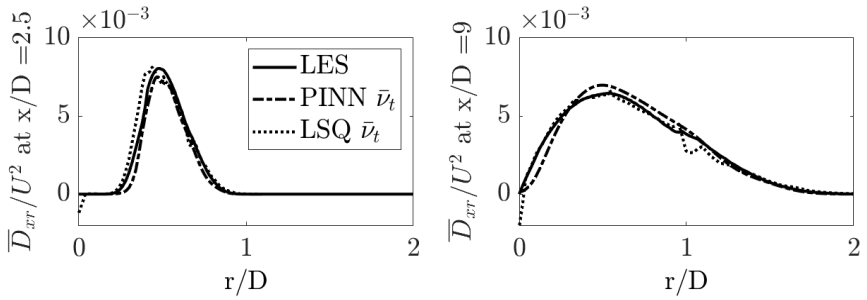

Fig. 3 Profiles of the normalized axial-radial component of the deviatoric part of the Reynolds stress tensor at x/D=2.5 (left) and x/D=9 (right). Components are computed based directly on the LES snapshots (solid), using the Boussinesq model and the PINN eddy viscosity (dashed) and using the LSQ eddy viscosity (dotted).

Figure 3 shows radial profiles of the axial-radial component of the modeled Reynolds stress tensor for both mean eddy viscosities at two axial locations (left $x/D = 2.5$, right $x/D = 9$). In addition the corresponding component directly computed based on the LES snapshots - axial-radial component of $\overline{\mathbf{u}'\mathbf{u}'}$ - (solid lines) is shown. It can be observed that both eddy viscosities approximate the axial-radial component dominant for the jet flow similarly well. Other components of the deviatoric part of the Reynolds stress tensor of minor importance to the mean momentum transfer [31], such as the axial-axial component, are poorly approximated by both eddy viscosities (not shown). The fact that the axial-radial component, which is dominant for the free jet, is similarly well approximated for both viscosities allows to draw two conclusions. First, the PINN-based assimilation procedure works fine, and second, the LSQ eddy viscosity is already a good approximation in terms of mean field consistency. This type of evaluation, which examines the closure model in isolation, is called a priori analysis. In the next section, the a priori analysis is performed for the coherent variables and the Boussinesq-like model.

B. A priori analysis

The idea of the a priori analysis is to evaluate a closure model in isolation. The methodology was applied, for example, in [32] to find a suitable linear model for heat release fluctuations as a function of fuel fluctuations in a turbulent jet flame. Here, different eddy viscosities are evaluated with respect to their potential to model the deviatoric part of the coherent Reynolds stress tensor according to the Boussinesq-like model, Eq. (8). To do this, the complex amplitudes of the harmonic velocity components (denoted with hat symbols) at a given frequency are obtained from the LES snapshots and inserted together with an eddy viscosity into the closure model, Eq. (8), which yields the modeled deviatoric part of the coherent Reynolds stress tensor $\widehat{\mathbf{D}}_\nu$ (Eqs. (8), (13) and (14)). In the a priori analysis, the modeled term is directly compared to the corresponding empirical term determined from the data, $\widehat{\mathbf{D}}_d$, which allows to assess the closure model in isolation.

For the stochastically forced (natural) jet data considered in this study, we determine the corresponding model inputs by means of SPOD and the validation data, $\widehat{\mathbf{D}}_d$, with the eSPOD as explained in Sec. III.B. It should be noted at this point that the empirical SPOD modes are subject to noise. This poses difficulties, since gradients of the velocity fluctuations have to be calculated to determine the coherent strain rate tensor $\widehat{\mathbf{T}}$, i.e. to evaluate the coherent Boussinesq-like model, Eq. (8).

Based on the SPOD coherent velocity modes and the eSPOD coherent Reynolds stress modes, different eddy viscosities for modeling the deviatoric part of the fluctuating Reynolds stress tensor are evaluated using the a priori analysis. In the scope of this study we consider three eddy viscosity models. First, we consider the LSQ eddy viscosity based on the Boussinesq inversion, Eq. (11), and the LES mean fields (lower half Fig. 2c). Second, the mean field consistent PINN eddy viscosity is considered (upper half Fig. 2c). For the first and second model, the fluctuating eddy viscosity term in Eq. (8) is neglected. In contrast, the third model takes into account the fluctuating part as well as the mean part. Both are computed using the PINN assimilated mixing length, Eq. (13) and (14). The second and third models therefore differ only in that the fluctuating component is taken into account in the third model.

The first row in Fig. 4 shows the real part of the axial-radial component of the coherent Reynolds stress tensor, $\widehat{\mathbf{D}}_d^{xr}$, determined with eSPOD at a frequency of St=0.47 and for three azimuthal orders. The first row thus shows the quantity to be modeled and can therefore be considered as validation. The second, third and fourth row show the corresponding modeled quantities, $\widehat{\mathbf{D}}_\nu^{xr}$, based on SPOD modes and the three eddy viscosity models.

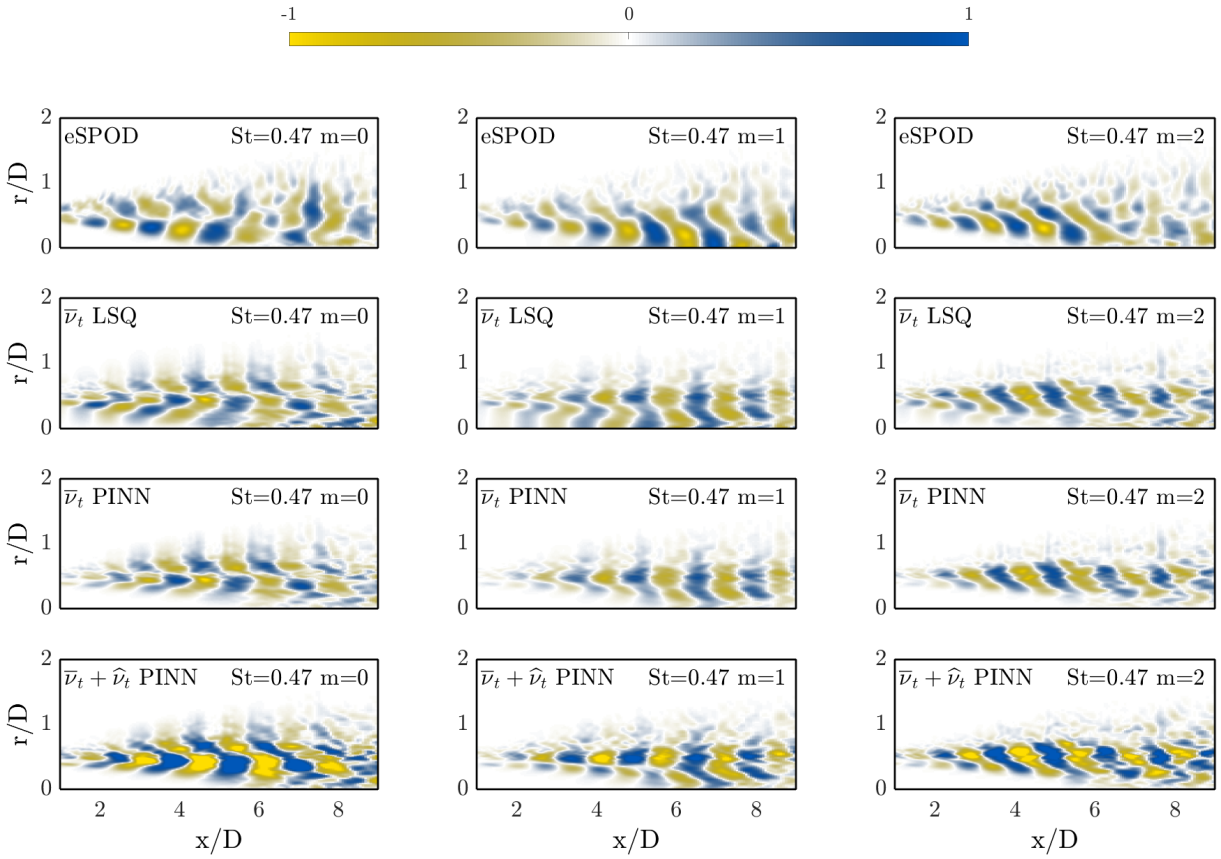

Fig. 4 Normalized axial-radial component of the coherent Reynolds stress tensor at St=0.47. From top to bottom: empirical using eSPOD, modeled with LSQ eddy viscosity, modeled with PINN mean eddy viscosity, modeld with mean and fluctuating PINN eddy viscosity. From left to right: m=0, 1 and 2. All modes of a given azimuthal order (each column) are normalized with the maximum value of the respective eSPOD mode.

Overall, a good qualitative agreement between the eSPOD (first row) and the modeled (second to fourth row) axial-radial coherent Reynolds stress component can be observed. For m=1 and 2 (second and third column) the agreement is better than for m=0 (first column). Comparing the result based on the LSQ eddy viscosity (second row) with the empirical eSPOD modes (first row), it becomes obvious that in the region of the potential core where the LSQ eddy viscosity is overestimated, the component of the coherent Reynolds stress tensor is also overestimated. In comparison, the model based on PINN eddy viscosity (third row) leads to a higher agreement with the eSPOD modes in this region. However, it can be observed for this model that the near-axis region with small values has a larger axial extent than seen in the validation data. Moreover, the PINN eddy viscosity model tends to underestimate the coherent Reynolds stress component for larger radii. The results of the third model (fourth row), which differs from the second model (third row) by taking into account the fluctuating eddy viscosity component, differ mainly in amplitude compared to the results of the second model. The mode shapes, however, are very similar. A comparison with the validation data shows that taking the fluctuating component into account (third vs. fourth row) leads to a poorer agreement.

For other frequencies in the low rank frequency range and also other components of the coherent Reynolds stress tensor, the results are similar (not shown). This leads us to conclude that the use of a fluctuating part of the eddy viscosity based on the linearized mixing length model is not advantageous for the case under consideration. The use of a mean eddy viscosity determined via the mean fields (LSQ or PINN) is sufficient to qualitatively represent the coherent Reynolds stress tensor. It should be noted that for the case considered, the mean field consistent PINN eddy viscosity model leads to slightly better results, which can be observed in the region of the potential core in Fig. 4.

Finally, this section explores the possibility of determining a mean eddy viscosity directly from the fluctuating

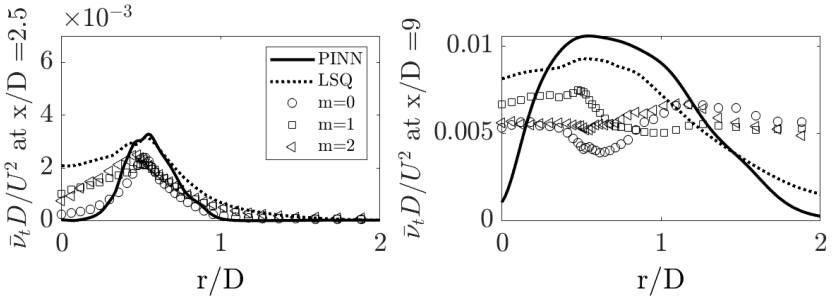

Fig. 5 Mean eddy viscosity profiles at two axial locations: left x/D=2.5, right x/D = 9. Linestyle and symbols indicate different models: PINN eddy viscosity (solid), LSQ eddy viscosity computed with Eq. (11) (dotted), absolute value of the eddy viscosity based on the inversion of the fluctuating Boussinesq-like model, Eq. (16) (markers). The marker shape denotes the azimuthal wave number. Results are averaged over the respective low rank frequency range (m=0 St=0.28-0.65, m=1 St=0.1-0.75, and m=2 St=0.1-0.65.).

quantities. As described in Section II.C, the Boussinesq-like model can be inverted, provided that the fluctuating eddy viscosity component is negligible, see Eq. (16). Thus, based on the coherent Reynolds stress tensor (eSPOD) and the coherent strain rate tensor (SPOD) an optimal eddy viscosity field can be determined in the least squares sense for each frequency. However, this approach poses a number of challenges. First, the modes are complex-valued and subject to noise. Since the equation requires the coherent strain rate tensor, gradients of the modes have to be computed which amplifies the noise of the SPOD modes. Moreover, it should be noted that the inversion of the Boussinesq equation in a least squares sense also by itself leads to noisy results. This is already the case with comparatively smooth input variables, such as for the mean field quantities, Eq. (11). To overcome these difficulties, we consider only the absolute value of the resulting eddy viscosity and also average over the corresponding low-rank frequency range for each azimuthal order considered, see red regions in Fig. 1. The resulting fields can thus be considered as optimal positive real-valued eddy viscosity fields for the considered frequency range.

Figure 5 compares the optimal viscosities calculated in this way for m=0, 1 and 2 against the PINN and LSQ mean eddy viscosities at two axial locations. Near the nozzle exit at x/D = 2.5 (left panel), it can be observed that the optimal eddy viscosities based on the coherent quantities agree well with the mean eddy viscosities. The agreement with the PINN eddy viscosity is slightly better, especially near the axis (small radii) and for m=0. This result is consistent with the observation that in the region of the potential core the PINN mean field consistent eddy viscosity is superior to the LSQ viscosity in representing the coherent Reynolds stress tensor, see Fig. 4. Further downstream, at x/D=9 (right panel in Fig. 5), the curves of the optimal eddy viscosities differ from the PINN and LSQ eddy viscosities. Although they are of the same order of magnitude, they show qualitative differences; while the LSQ and PINN eddy viscosities show a pronounced structure with high values for medium, and decreasing values for small and large radii, the curves for the optimal eddy viscosities determined directly from the coherent quantities appear to fluctuate around a spatially constant value of approximately 0.005. This value is approximately half of the maximum value of the PINN and LSQ curves. Since the curves are qualitatively different, it is difficult to judge in this region whether the PINN or the LSQ eddy viscosity better approximates the optimal eddy viscosities. Overall, however, the LSQ eddy viscosity is closer to the m=0, 1 and 2 optimal curves.

In summary, the results of the a priori analysis show that the terms to be closed in the coherent transport equations can be approximated by a Boussinesq-like model. For the considered case, the consideration of a mean eddy viscosity field is sufficient. This was also confirmed by inverting the Boussinesq-like model based on the coherent quantities. Thus, it was possible to calculate the eddy viscosities that best approximate the coherent Reynolds stress tensor based on the coherent strain rate tensor in the least squares sense. Based purely on a real valued analysis (only considering the absolute value), the PINN and LSQ eddy viscosity were found to be of the correct order of magnitude and even to match the desired curve near the nozzle exit.

C. A posteriori analysis

The closure model, inserted in the linear operator, allows the calculation of stability modes using linear stability analysis or of forcing and response modes using resolvent analysis. These modes can be compared to experimentally observed coherent structures, which is known as a posteriori analysis of the linearized mean field operator. More

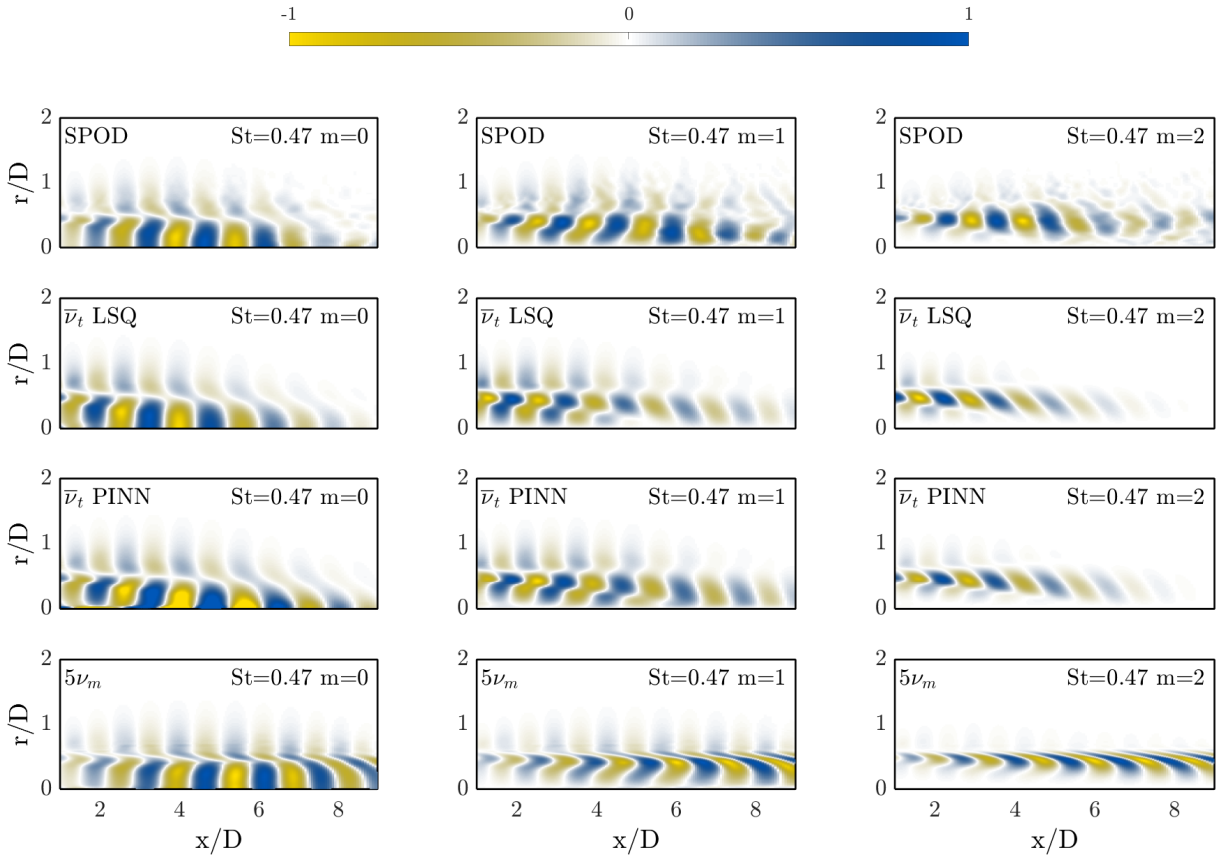

Fig. 6 Normalized real part of the axial velocity component at St=0.47. From top to bottom: SPOD, resolvent with LSQ eddy viscosity, resolvent with PINN eddy viscosity, resolvent with 5 times the molecular viscosity. From left to right: m=0, 1 and 2. Each SPOD and $5\nu_m$ mode is normalized with its respective maximum value. The LSQ and PINN modes are normalized using the maximum value of the LSQ mode for each respective azimuthal order.

specifically, in this study we are interested in using resolvent analysis to model the dominant coherent structures that we observe with SPOD in the natural flow. To compute resolvent modes, we use the in-house finite element code FELiCS [32, 33]. Since the a priori analysis did not reveal any advantages for a fluctuating eddy viscosity model, we use only the two mean eddy viscosity fields, LSQ and PINN. As a reference case, we also consider a case without eddy viscosity, but with five times increased spatially constant molecular viscosity, $5\nu_m = 10^{-4}$. This value is two orders of magnitude lower than the maximum value of the PINN and LSQ eddy viscosity, see Fig. 5.

Figure 6 shows the real part of the axial velocity fluctuation at St=0.47 from left to right for m=0, 1 and 2. The first row shows the real part of the SPOD modes, the validation quantity to be modeled with the resolvent analysis. Rows 2 to 4 show the corresponding real parts of the resolvent modes for the LSQ, PINN, and $5\nu_m$ viscosity. As expected, the reference case (fourth row), which is based solely on a spatially constant viscosity of the order of the molecular one, exhibits the largest deviations compared to the SPOD modes. For m=0 (first column) qualitative agreement is still found, for m=1 (second) and m=2 (third column) the results differ substantially. Considering the results of the LSQ and PINN eddy viscosity resolvent modes (second and third row), hardly any differences can be observed between the two. Moreover, both show a very high agreement with the SPOD modes for all three azimuthal orders. This result was also to be expected, since both models perform similarly well in the a priori analysis, Fig. 4 and qualitatively reproduce the optimal viscosity fields shown in Fig. 5.

However, a detailed inspection of the potential core region, where differences were also observed in the a priori analysis, also reveals small differences between the LSQ and PINN resolvent modes (second and third row). The PINN

eddy viscosity in this region is considerably lower than the LSQ eddy viscosity, Fig. 2c, which affects the shape of the resolvent modes. For m=0, the mean field consistent PINN eddy viscosity appears to be too low in this region, which is evident from the mode shape (first column, third row) in the immediate vicinity of the axis. In contrast, for m=1, but also for m=2, the mean field consistent PINN eddy viscosity leads to slightly better results in this region compared to the LSQ viscosity, which appears to be too dissipative.

In summary, the a posteriori analysis confirms a previously known finding [2, 14, 16, 23]: the inclusion of a Boussinesq-like eddy viscosity model to approximate the coherent Reynolds stress fluctuations improves the modeling of coherent structures based on resolvent analysis. A particularly high agreement between the resolvent and SPOD modes is observed when the eddy viscosity is determined from the mean velocity fields. For the considered azimuthal modes (m=1 and m=2), the mean field consistent PINN eddy viscosity leads to slightly better results compared to the LSQ eddy viscosity determined by inversion of the Boussinesq equation, Eq. (11).

V. Conclusion

The transport equations for coherent structures contain an unknown term, the coherent part of the Reynolds stress tensor. The most popular closure model is a Boussinesq-like model that relates the deviatoric part of the coherent Reynolds stress tensor to the coherent strain rate tensor via an eddy viscosity. In this study, we propose the concept of self-consistency in the closure problem, meaning that the eddy viscosity together with the mean field quantities approximate a solution of the RANS equation. The resulting eddy viscosity field can be considered mean field consistent. The mean field consistency is achieved by assimilating the eddy viscosity using a PINN that takes into account both the approximation of the mean field and the RANS equations. If the eddy viscosity is not assimilated directly, but the constants of an eddy viscosity model are assimilated, fluctuations of the eddy viscosity can also be accounted for in the transport equations of the coherent structures via a linearization of the eddy viscosity model around the mean field.

Considering a natural jet flow at Re=50000 and Ma=0.4, different eddy viscosities are studied according to their potential to model the closure term. For this purpose, the coherent strain rate tensor is determined via SPOD and the deviatoric part of the coherent Reynolds stress tensor is determined via eSPOD, which allows a qualitative and quantitative evaluation of the closure model. This analysis of the closure model in isolation is called a priori analysis. It is shown that the Boussinesq-like closure model provides a good approximation of the coherent component of the Reynolds stress tensor. Compared to a mean eddy viscosity derived from the inversion of the Boussinesq model (LSQ), the PINN mean field consistent eddy viscosity shows better results in the region of the potential core. However, with the exception of this region, the results are very similar, which is due to the fact that the eddy viscosities are also very similar. Including a fluctuating eddy viscosity component based on the linearization of the mixing length model does not bring any advantages; on the contrary, the fluctuating eddy viscosity even leads to an overestimation of the amplitude of the coherent Reynolds stresses.

Based on the coherent quantities, the Boussinesq-like model can also be inverted, and thus an optimal mean eddy viscosity can be determined in the least squares sense for each azimuthal order considered. A comparison with the LSQ and PINN eddy viscosity shows what was already to be expected from the a priori analysis: the mean eddy viscosities are in the same order of magnitude as the absolute value (averaged over low-rank frequency range) of the optimal eddy viscosities. In the upstream region of the flow, near the nozzle (x/D=2.5), even the quantitative agreement is high. These results provide new insights into the modeling of the closure term of the coherent transport equations. In particular, the results show why the Boussinesq-like closure model improves the results of linear analyses: via mean eddy viscosity, the coherent Reynolds stress components can be approximated by the coherent strain rate tensor.

In the last part of the study, we show that the PINN and LSQ eddy viscosities also lead to resolvent modes that fit very well to the SPOD validation modes. This comparison is called a posteriori analysis in analogy to the a priori analysis. The axial velocity mode shapes of the resolvent modes based on PINN and LSQ eddy viscosity differ slightly in the region of the potential core, in which the eddy viscosities differ substantially. For the considered axial velocity component, it is shown for m=1 and 2 that the mean field consistent PINN eddy viscosity leads to slightly better results, whereas the LSQ eddy viscosity overestimates the dissipation in this region.

In summary, this study provides tools to build and investigate closure models for the transport equations of coherent structures. With the PINN approach, a method is presented to find a turbulent viscosity field consistent with the mean field that is suitable for the linear modeling. In contrast to other commonly applied methods, the approach requires only the mean fields and no further information about the turbulent statistics.

Acknowledgments

We gratefully acknowledge the Deutsche Forschungsgemeinschaft (DFG) for funding this work within the projects 441269395 and 506170981. Furthermore, we would like to thank the German Ministry of Economic Affairs and Climate Action as well as MAN Energy Solutions SE for funding this project within the scope of AG Turbo (ROBOFLEX 03EE5013E). We also thank Miriam Goldack for her help with the resolvent analysis.

References

[1] Barkley, D., "Linear analysis of the cylinder wake mean flow," *EPL (Europhysics Letters)*, Vol. 75, No. 5, 2006, p. 750. https://doi.org/https://doi.org/10.1209/epl/i2006-10168-7.

[2] Tammisola, O., and Juniper, M. P., "Coherent structures in a swirl injector at Re = 4800 by nonlinear simulations and linear global modes," *Journal of Fluid Mechanics*, Vol. 792, 2016, pp. 620–657. https://doi.org/10.1017/jfm.2016.86.

[3] Terhaar, S., Oberleithner, K., and Paschereit, C., "Key parameters governing the precessing vortex core in reacting flows: An experimental and analytical study," *Proceedings of the Combustion Institute*, Vol. 35, No. 3, 2015, pp. 3347 – 3354. https://doi.org/http://dx.doi.org/10.1016/j.proci.2014.07.035.

[4] Casel, M., Oberleithner, K., Zhang, F., Zirwes, T., Trimis, D., Bockhorn, H., and Kaiser, T., "Resolvent-based Modelling of Coherent Structures in a Turbulent Jet Flame Using a Passive Flame Approach," *Combustion and Flame*, Vol. 90, 2021, p. 111695. https://doi.org/10.1016/j.combustflame.2021.111695.

[5] Emerson, B., Lieuwen, T., and Juniper, M. P., "Local stability analysis and eigenvalue sensitivity of reacting bluff-body wakes," *Journal of Fluid Mechanics*, Vol. 788, 2016, pp. 549–575. https://doi.org/10.1017/jfm.2015.724.

[6] Hemchandra, S., Shanbhogue, S., Hong, S., and Ghoniem, A. F., "Role of hydrodynamic shear layer stability in driving combustion instability in a premixed propane-air backward-facing step combustor," *Physical Review Fluids*, Vol. 3, No. 6, 2018. https://doi.org/10.1103/physrevfluids.3.063201.

[7] Demange, S., Qadri, U., Juniper, M., and Pinna, F., "Global modes of viscous heated jets with real gas effects," *Journal of Fluid Mechanics*, Vol. 936, 2022, p. A7. https://doi.org/10.1017/jfm.2022.43.

[8] Schmidt, O. T., Towne, A., Rigas, G., Colonius, T., and Brès, G. A., "Spectral analysis of jet turbulence," *Journal of Fluid Mechanics*, Vol. 855, 2018, pp. 953–982. https://doi.org/10.1017/jfm.2018.675.

[9] Abreu, L. I., Cavalieri, A. V., and Wolf, W., "Coherent hydrodynamic waves and trailing-edge noise," *23rd AIAA/CEAS Aeroacoustics Conference*, 2017, p. 3173. https://doi.org/10.2514/6.2017-3173.

[10] Sano, A., Abreu, L. I., Cavalieri, A. V., and Wolf, W. R., "Trailing-edge noise from the scattering of spanwise-coherent structures," *Physical Review Fluids*, Vol. 4, No. 9, 2019, p. 094602. https://doi.org/10.1103/PhysRevFluids.4.094602.

[11] Wagner, G. A., Deuse, M., Illingworth, S. J., and Sandberg, R. D., "Resolvent analysis-based pressure modeling for trailing edge noise prediction," *25th AIAA/CEAS Aeroacoustics Conference*, 2019, p. 2720. https://doi.org/10.2514/6.2019-2720.

[12] Pasche, S., Avellan, F., and Gallaire, F., "Part load vortex rope as a global unstable mode," *Journal of Fluids Engineering*, Vol. 139, No. 5, 2017. https://doi.org/10.1115/1.4035640.

[13] Müller, J. S., Sieber, M., Litvinov, I., Shtork, S., Alekseenko, S., and Oberleithner, K., "Prediction of vortex precession in the draft tube of a model hydro turbine using mean field stability theory and stochastic modelling," *IOP Conference Series: Earth and Environmental Science*, Vol. 774, IOP Publishing, 2021, p. 012003. https://doi.org/10.1088/1755-1315/774/1/012003.

[14] Pickering, E., Rigas, G., Schmidt, O. T., Sipp, D., and Colonius, T., "Optimal eddy viscosity for resolvent-based models of coherent structures in turbulent jets," *Journal of Fluid Mechanics*, Vol. 917, 2021. https://doi.org/10.1017/jfm.2021.232.

[15] Kuhn, P., Soria, J., and Oberleithner, K., "Linear modeling of self-similar jet turbulence," *Journal of Fluid Mechnanics*, , No. A7, 2021. https://doi.org/10.1017/jfm.2021.292.

[16] Kuhn, P., Müller, J. S., Knechtel, S., Soria, J., and Oberleithner, K., "Influence of eddy viscosity on linear modeling of self-similar coherent structures in the jet far field," *AIAA SCITECH 2022 Forum*, 2022, p. 0460. https://doi.org/10.2514/6.2022-0460.

[17] Symon, S., Illingworth, S. J., and Marusic, I., "Energy transfer in turbulent channel flows and implications for resolvent modelling," *Journal of Fluid Mechanics*, Vol. 911, 2021, p. A3. https://doi.org/10.1017/jfm.2020.929.

[18] Symon, S., Madhusudanan, A., Illingworth, S. J., and Marusic, I., "On the use of eddy viscosity in resolvent analysis of turbulent channel flow," *arXiv preprint arXiv:2205.11216*, 2022. https://doi.org/https://doi.org/10.48550/arXiv.2205.11216.

[19] Crouch, J., Garbaruk, A., and Magidov, D., "Predicting the onset of flow unsteadiness based on global instability," *Journal of Computational Physics*, Vol. 224, No. 2, 2007, pp. 924–940. https://doi.org/https://doi.org/10.1016/j.jcp.2006.10.035.

[20] Viola, F., Iungo, G. V., Camarri, S., Porté-Agel, F., and Gallaire, F., "Prediction of the Hub Vortex Instability in a Wind Turbine Wake: Stability Analysis with Eddy-Viscosity Models Calibrated on Wind Tunnel Data," *Journal of Fluid Mechanics*, Vol. 750, 2014. https://doi.org/10.1017/jfm.2014.263.

[21] Towne, A., Schmidt, O. T., and Colonius, T., "Spectral proper orthogonal decomposition and its relationship to dynamic mode decomposition and resolvent analysis," *Journal of Fluid Mechanics*, Vol. 847, 2018, p. 821–867. https://doi.org/10.1017/jfm.2018.283.

[22] Reynolds, W. C., and Hussain, A. K. M. F., "The Mechanics of an Organized Wave in Turbulent Shear Flow. Part 3. Theoretical Models and Comparisons with Experiments," *Journal of Fluid Mechanics*, Vol. 54, No. 2, 1972, pp. 263–288. https://doi.org/10.1017/S0022112072000679.

[23] Rukes, L., Paschereit Oliver, C., and Oberleithner, K., "An assessment of turbulence models for linear hydrodynamic stability analysis of strongly swirling jets," *European Journal of Mechanics - B/Fluids*, Vol. 59, 2016, pp. 205–218. https://doi.org/10.1016/j.euromechflu.2016.05.004.

[24] Pope, S. B., and Pope, S. B., *Turbulent flows*, Cambridge university press, 2000. https://doi.org/10.1017/CBO9780511840531.

[25] von Saldern, J. G. R., Reumschüssel, J. M., Kaiser, T. L., Sieber, M., and Oberleithner, K., "Mean flow data assimilation based on physics-informed neural networks," *Physics of Fluids*, Vol. 34, No. 11, 2022. https://doi.org/10.1063/5.0116218.

[26] Raissi, M., Perdikaris, P., and Karniadakis, G. E., "Physics-informed neural networks: A deep learning framework for solving forward and inverse problems involving nonlinear partial differential equations," *Journal of Computational Physics*, Vol. 378, 2019, pp. 686–707. https://doi.org/https://doi.org/10.1016/j.jcp.2018.10.045.

[27] Brès, G. A., Ham, F. E., Nichols, J. W., and Lele, S. K., "Unstructured Large-Eddy Simulations of Supersonic Jets," *AIAA Journal*, Vol. 55, No. 4, 2017, pp. 1164–1184. https://doi.org/10.2514/1.J055084.

[28] Brès, G. A., Jordan, P., Jaunet, V., Le Rallic, M., Cavalieri, A. V. G., Towne, A., Lele, S. K., Colonius, T., and Schmidt, O. T., "Importance of the nozzle-exit boundary-layer state in subsonic turbulent jets," *Journal of Fluid Mechanics*, Vol. 851, 2018, p. 83–124. https://doi.org/10.1017/jfm.2018.476.

[29] Maia, I. A., Jordan, P., Cavalieri, A. V. G., Martini, E., Sasaki, K., and Silvestre, F. J., "Real-time reactive control of stochastic disturbances in forced turbulent jets," *Physical Review Fluids*, Vol. 6, No. 12, 2021, p. 123901. https://doi.org/10.1103/PhysRevFluids.6.123901.

[30] Nekkanti, A., Maia, I., Jordan, P., Heidt, L., Colonius, T., , and Schmidt, O. T., "Triadic nonlinear interactions and acoustics of forced versus unforced turbulent jets," *Twelveth International Symposium on Turbulence and Shear Flow Phenomena (TSFP12)*, Osaka, Japan (Online), July 19-22, 2022.

[31] Rajaratnam, N., *Turbulent jets*, Elsevier, 1976.

[32] Kaiser, T. L., Varillon, G., Polifke, W., Zhang, F., Zirwes, T., Bockhorn, H., and Oberleithner, K., "Modelling the response of a turbulent jet flame to acoustic forcing in a linearized framework using an active flame approach," *Combustion and Flame*, Vol. 253, 2023, p. 112778. https://doi.org/https://doi.org/10.1016/j.combustflame.2023.112778.

[33] Kaiser, T. L., and Oberleithner, K., "A Global Linearized Framework for Modelling Shear Dispersion and Turbulent Diffusion of Passive Scalar Fluctuations," *Journal of Fluid Mechnanics*, , No. A111, 2021. https://doi.org/doi:10.1017/jfm.2021.151.